energies

MDPI

Article

Natural Convection Effect on Solidification Enhancement in a Multi-Tube Latent Heat Storage System: Effect of Tubes' Arrangement

Mohammadreza Ebrahimnataj Tiji [1], Jasim M. Mahdi [2], Hayder I. Mohammed [3], Hasan Sh. Majdi [4], Abbas Ebrahimi [5], Rohollah Babaei Mahani [6], Pouyan Talebizadehsardari [7,*] and Wahiba Yaïci [8,*]

[1] Department of Mechanical Engineering, Qom University of Technology, Qom 3718146645, Iran; ebrahimnataj.m@qut.ac.ir
[2] Department of Energy Engineering, University of Baghdad, Baghdad 10071, Iraq; jasim@siu.edu
[3] Department of Physics, College of Education, University of Garmian, Kurdistan, Kalar 46021, Iraq; hayder.i.mohammad@garmian.edu.krd
[4] Department of Chemical Engineering and Petroleum Industries, Al-Mustaqbal University College, Babylon 51001, Iraq; hasanshker1@gmail.com
[5] School of Mechanical Engineering, Babol Noshirvani University of Technology, Babol 4714871167, Iran; abbasebrahimi70@yahoo.com
[6] Belmore Energy Ltd., Edgware HA8 7EB, UK; rbmahani@gmail.com
[7] Centre for Sustainable Energy Use in Food Chains, Institute of Energy Futures, Brunel University London, Kingston Lane, Uxbridge, Middlesex UB8 3PH, UK
[8] CanmetENERGY Research Centre, Natural Resources Canada, 1 Haanel Drive, Ottawa, ON K1A 1M1, Canada
* Correspondence: pouyan.talebizadehsardari@brunel.ac.uk (P.T.); wahiba.yaici@canada.ca (W.Y.)

Citation: Tiji, M.E.; Mahdi, J.M.; Mohammed, H.I.; Majdi, H.S.; Ebrahimi, A.; Mahani R.B.; Talebizadehsardari, P.; Yaïci, W. Natural Convection Effect on Solidification Enhancement in a Multi-Tube Latent Heat Storage System: Effect of Tubes' Arrangement. *Energies* **2021**, *14*, 7489. https://doi.org/10.3390/en14227489

Academic Editors: Valerio D'Alessandro and Adrián Mota Babiloni

Received: 11 September 2021
Accepted: 1 November 2021
Published: 9 November 2021

Publisher's Note: MDPI stays neutral with regard to jurisdictional claims in published maps and institutional affiliations.

Abstract: The solidification process in a multi-tube latent heat energy system is affected by the natural convection and the arrangement of heat exchanger tubes, which changes the buoyancy effect as well. In the current work, the effect of the arrangement of the tubes in a multi-tube heat exchanger was examined during the solidification process with the focus on the natural convection effects inside the phase change material (PCM). The behavior of the system was numerically analyzed using liquid fraction and energy released, as well as temperature, velocity and streamline profiles for different studied cases. The arrangement of the tubes, considering seven pipes in the symmetrical condition, are assumed at different positions in the system, including uniform distribution of the tubes as well as non-uniform distribution, i.e., tubes concentrated at the bottom, middle and the top of the PCM shell. The model was first validated compared with previous experimental work from the literature. The results show that the heat rate removal from the PCM after 16 h was 52.89 W (max) and 14.85 W (min) for the cases of uniform tube distribution and tubes concentrated at the bottom, respectively, for the proposed dimensions of the heat exchanger. The heat rate removal of the system with uniform tube distribution increases when the distance between the tubes and top of the shell reduces, and increased equal to 68.75 W due to natural convection effect. The heat release rate also reduces by increasing the temperature the tubes. The heat removal rate increases by 7.5%, and 23.7% when the temperature increases from 10 °C to 15 °C and 20 °C, respectively. This paper reveals that specific consideration to the arrangement of the tubes should be made to enhance the heat recovery process attending natural convection effects in phase change heat storage systems.

Keywords: natural convection; phase change material; tubes' arrangement; thermal energy storage; solidification; multi-tubes heat exchanger

1. Introduction

Comprehensive socio-economic changes are coupled with higher requirements of major energy sources, while the global demand for energy supply have increased by 1.5 times due to industrial developments [1,2]. Fossil fuels as the primary resources, which provides 80% of the major power, have been reduced, on account of an increase in clean energy usage because of reducing raw resources and climate change, which is caused by the emission of harmful gases and particles [3,4]. The innovation of a high-efficiency technology to utilize a renewable energy resource is highly promising [5,6]. The erratic and unexpected behavior of renewable energy sources have a negative impact in extensive applications [7]. Thermal energy storage (TES) systems are considered a critical solution to eliminate the gap between energy supply and demand. Latent, sensible, and thermochemical heat are the presented formations for saving energy in TES systems [8]. Latent heat storage (LHS) employs phase-change materials (PCM) to absorb and release thermal energy through the phase changes between solid and liquid under almost constant temperature conditions. The advantages of PCMs are a high heat capacity, low environmental risks, and operating in a very narrow range of temperature [9–11]. Generally, the weak thermal conductivity of PCMs, which range from 0.1 to 0.8 W/(m·K) [12], reduces the phase change rates, which causes a limitation of their applications. Therefore, several thermal efficiency improvement methods have been developed and applied to improve the heat transfer rate in the system [13,14]. These methods include adding fins and extended surfaces [15,16], modifying the geometry [17–20], porous media [21–24], heat tubes [25–28], composing thermally high conducting particles [29,30], multiple PCMs [31,32], nanoparticles [33,34], and using the combinations of different methods [35–37]. To enhance the natural convection in the system, multi-HTF tubes could be used, which is also valuable regarding the weight and cost of the design [38,39].

In the state of geometrical designs, there are two categories: shell and tube systems [40–43] and triple homocentric tube [44,45] units. The shell and tube thermal exchanger combined with extended surfaces is an ideal case because of the high heat transfer performance, its simple design, and its easier combination in applications. This unit is based on the PCM's position and the number and location of tubes, which are also categorized into several types, including pipe, cylinder, and multi-tube [46]. In the tube mode, the PCM is inside the tube and the HTF flows over the external wall. In the cylinder mode [47], which is considered as the ideal shell-tube configuration, the HTF flows inside the pipes, and the PCM is surrounded by the shell. Pakalka et al. [48] experimentally and theoretically studied the natural convection heat transfer in the PCM-based fin and tube thermal exchanger. They found that the convection heat transfer coefficient was equal to 61 and 68 W/m^{2}K in the experimental and theoretical methods, respectively. Mahdi et al. [32] studied the thermal reaction of the shell-and-tube TES consisting of multiple segments carrying separate PCMs of different phase-change points. They found that applying multi-segments increases the phase-change rate up to 94%. Rathod and Banerjee [49] studied both phase-change rates of PCM in vertical shells and tubes. They found that the phase-change rate, with and without three longitudinal extended fins, was improved by 25% and 44%, respectively. Lohrasbi et al. [50] stated that the combination of the fins enhances the melting rate in the vertical shell and tube by 3.3-, 3.6-, and 4.3-fold compared with the finless case. Esapour et al. [51] theoretically studied the optimization of the number and the diameter of the multiple-tube system. They found that the melting rate improves by 29% when a system with four tubes is applied, compared with a single tube unit, and they also found that the tube located at the bottom part of the system enhances the performance. Rabienataj Darzi et al. [52] reported that the phase change rate improves with adding fins to the system of shell and tube. They stated that the melting and solidification rate increase by 39 to 82% and 28 to 85% when the number of the fins rose from 4 to 20. Khan et al. [53] developed a new shape of shell and tube combined with a longitudinal fin. They found that raising the inlet temperature from 323 to 343 K considerably enhanced the phase change rate and total enthalpy by 69% and 18%, respectively.

Numerous studies have been attained to improve the discharging process [54–57]. The first numerical study examining the discharging process was conducted by Tao [58]. He formed a model to detect the interface shifting procedure through the phase-change process. Gortych et al. [59] experimentally and numerically evaluated the solidification process of the PCM placed in a horizontal annular tube. A constant wall temperature was assumed, and a normal range of the free convection coefficient was detected. Abdollahzadeh and Esmaeilpour [60] evaluated the wavy wall TES, combined with a nanofluid as HTF. A considerable impact on the thermal efficiency of the unit was detected due to applying a special configuration and nanofluid as HTF. Shahsavar et al. [61] explored the impact of the wavy channel and the porous medium on the TES. They found that the unit design and the metal foam have a significant impact on the thermal operation of the discharging process because of increasing the thermal exchange surface area and improving the mean thermal conductivity of the unit. Choi and Kim [62] assessed the round fins for the solidification enhancement in the LHS. They indicated that the fins enhance the thermal coefficient 3 fold over the finless case. Wang et al. [63] numerically analyzed the discharging process in a zigzag configuration heat exchanger. A considerable impact on the heat transfer efficiency has been noticed due to the average velocity of the HTF. Sardari et al. [19] examined the modified zigzag design of the LHS. They stated that the system with a zigzag angle of 60° decelerates the storage rate by 1/3 times over the rate of the situation with a 30° zigzag angle.

The optimization of the variable dependent factors to achieve a higher efficiency, lower cost, and smaller size have been studied by several researchers. Bazai et al. [27] studied the thermal optimization of the circular elliptical double pipe-based TES unit. They detected the optimum values of the diameters of the pipes and the angular position. They found that the wider angle of the channel produced a faster charging rate, the melting rate increased by 61%, and the performance enhanced by 26% when the aspect ratio (hydraulic diameter to the length of the tubes) was 0.33 compared with the aspect ratio of 1. Talebzadehsardari et al. [36] analyzed the optimum shape and location of airflow pipes on the discharging process of a combined metal foam-PCM unit. They found that the solidification time dropped by 57%, and the temperature difference between both ends of the discharging rate improved by three times compared with the unit with the straight air tube. Li et al. [64] mathematically studied the optimization of the packed-bed TES with cascaded PCM capsules under the constraints of outlet threshold temperature. They found that the effective usage rate can achieve 84%, which is about twice as high as that in non-cascaded PCM-TES. Liang et al. [65] studied the performance optimization for shell-and-tube PCM thermal energy storage. The fully turbulent flow strongly improves the melting rate 50 fold and raises the capacity efficiency at the applied PCM volume ratio from 0.2–0.8 to 0.6–0.9 at laminar flow cases.

The literature review shows that there are many parameters that could be important factors in the discharging process of PCM. The location of the tubes (HTF channels) has a considerable impact on the movement of the liquid PCM and the thermal efficiency of the unit. Studying and optimizing the position of the multi-tube provides better information and knowledge in this field. Therefore, the current work, with the novel idea, aimed to scientifically optimize and design the efficiency of a shell-and-tube LHTES to increase the solidification rate and improve the thermal rate from the PCM to the HTF. The lowest distance between the upper tube and the top wall was optimized to gain the lowest solidification time. The evaluation was achieved by analyzing the liquid fraction (LF), the solidification rate, the contours of the phases, and the temperature. It should be noted that the melting process of the proposed heat exchanger has been studied previously by the authors [3]. This paper is focused on the heat recovery process as the effect of natural convection and buoyancy for various arrangements of the tubes are completely different when compared with the melting process, which is studied separately in this paper. The aim was to move the HTF tubes' location through the PCM area to reach the best location and take full benefit of free convection flows to reduce the discharging time.

2. Problem Description

The investigated system is a multi-tube shell-and-tube heat exchanger, incorporating several tubes in a rectangular PCM container. Figure 1a illustrated the schematic of the proposed heat exchanger incorporating seven tubes in symmetrical conditions from both the left and right sides that could be extended by repeating the pattern in the horizontal direction, and Figure 1b illustrates the full domain. This assumption can be considered with a long width for the heat exchanger. The heat exchanger's upper and lower walls are adiabatic to eliminate the impact of environmental conditions with no-slip boundary conditions. Different tubes' wall temperatures of 10, 15, and 20 °C are considered for the solidification process, while the initial temperature of the PCM is equal to 50 °C. Gravity is considered in the vertical direction toward the bottom of the heat exchanger. It should be noted that the system is studied in two-dimensional conditions due to the high computational cost of 3D simulations. It should be noted that this assumption is meaningful considering a long length of the heat exchanger ignoring the wall effects.

The nominal diameter of the tube (D) is 12.7 mm (0.5 in) with an outer diameter of 15.875 mm, which is one of the standard sizes of copper tubes in heat exchangers. The height of the shell is assumed to be 314.325 mm, and the width of each repeated section is considered to be 71.344 mm. As shown in Figure 1a, for the uniform distribution of the pipes, it is assumed that the distance between two pipes that are next to each other on the left wall and the adjacent pipe on the right wall is constant. In addition, the tubes on the right-hand side of the shell are located at the center line of the two adjacent tubes on the left-hand side wall. In other words, the centers of these pipes generate an equilateral triangle for the uniform arrangement of the pipes. The reason for using a staggered array of the pipes is a better and more uniform distribution of the heat sinks (pipes with low temperature) in the heat exchangers, considering a constant number of the tubes. Thus, during the solidification process, a heat sink can fill the gap between the two adjacent pipes in the vertical direction, which can help improve the solidification rates of the heat exchanger. It should be noted that different arrangements are defined to evaluate the effect of natural convection in the proposed shell and tube heat exchanger, which are presented later in the results and discussion sections.

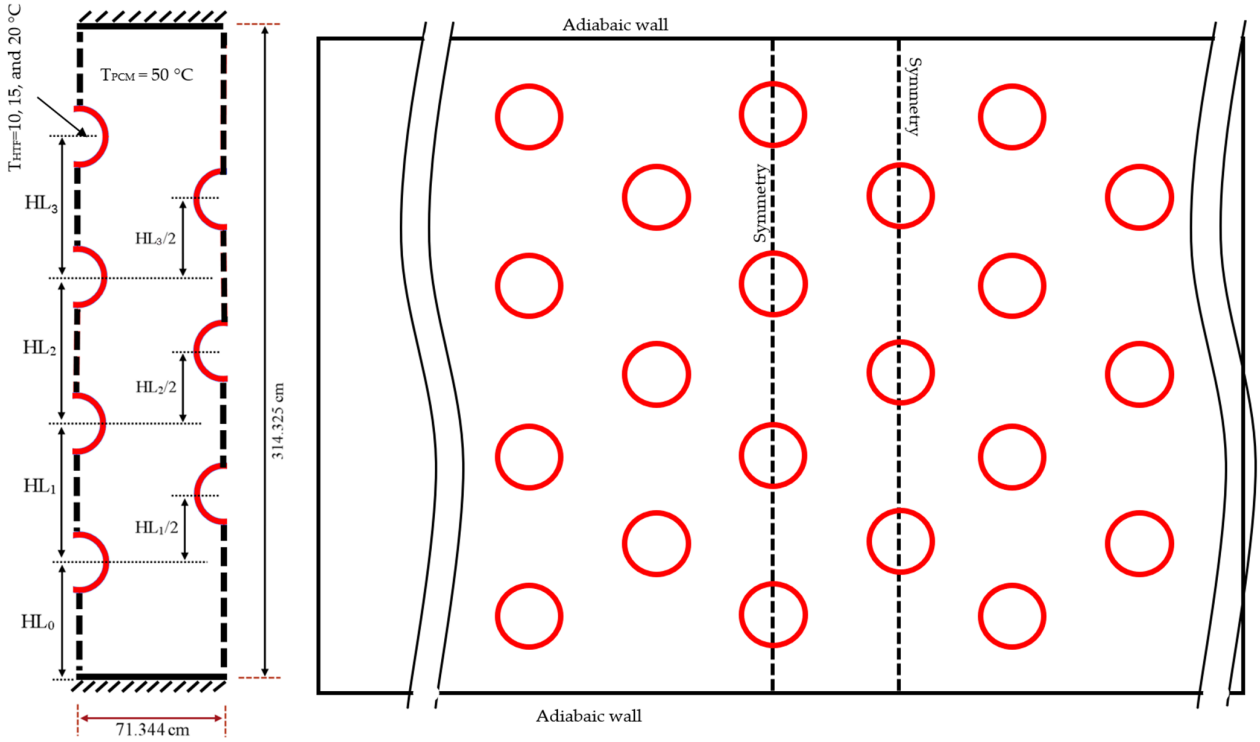

Figure 1. The schematic of the studied multiple heat exchanger: (**a**) symmetry condition, (**b**) full domain.

RT-35 is used as the PCM in this study, of which the thermo-physical properties are presented in Table 1. The density is assumed to be constant because the specific mass of the PCM is contained in the same volume (constant mass and constant volume), and then the density is constant even during the solidification process.

Table 1. Thermophysical properties of RT35 [66].

Property	RT35
Specific heat (kJ/kgK)	2
Viscosity (Pas)	0.023
Heat of fusion (kJ/kg)	170
Liquidus temperature (°C)	35
Density (kg/m^3)	815
Thermal conductivity (W/mK)	0.2
Solidus temperature (°C)	29
Thermal expansion coefficient (1/K)	0.0006

3. Mathematical Modeling

The governing equation in this case for 2D laminar, incompressible, transient, and Newtonian fluid flow are provided as follows, built on the enthalpy-porosity technique defined by Brent et al. [67] considering the assumptions of employing a Boussinesque approximation for natural convection effects due to low-temperature variation in the domain [67], and neglecting viscous dissipation because of the non-appearance of high velocities [67]:

$$\frac{\partial \rho}{\partial t} + \nabla . \rho \vec{V} = 0 \quad (1)$$

$$\frac{\partial \rho}{\partial t} + \nabla . \rho \vec{V} = 0 \quad (2)$$

$$\frac{\partial (\rho v)}{\partial t} + \nabla \cdot \left(\rho v \vec{V}\right) = -\frac{\partial P}{\partial y} + \nabla \cdot (\mu \nabla v) - \rho g \beta \left(T - T_{ref}\right) - \frac{A_m (1-\beta^2)}{\lambda^3 + 0.001} v \quad (3)$$

$$\rho C_p \frac{\partial T}{\partial t} + \rho C_p \nabla \left(\vec{V} T\right) = \nabla (k \nabla T) - \left[\nabla \left(\rho \vec{V} \lambda L_f\right) + \frac{\partial \rho \lambda L_f}{\partial t}\right]$$

where A_m is the mushy constant which is selected as 105, following [42]. The symbol λ shows the liquid volume fraction (melted fraction of PCM in an element), defined as:

$$\lambda = \frac{\Delta H}{L_f} = \begin{Bmatrix} 0 if T < T_S \\ \frac{(T - T_S)}{(T_L - T_S)} if T_S < T < T_L \\ 1 if T > T_L \end{Bmatrix}, \quad (4)$$

where the total enthalpy of an element is the combination of latent heat (ΔH) and sensitive enthalpy (h) as $H = \Delta H + h$. Thus, the total enthalpy could be computed by the integration of H over the computational domain.

The solidification or discharging rate $\dot{Q}$ is introduced as [68]:

$$\dot{Q} = \frac{Q}{t_m} = \frac{m\left(\int_S C_p dT + L_f + \int_L C_p dT\right)}{t_m}, \quad (5)$$

where t_m is the melting time and m is the mass of PCM.

4. Numerical Process

ANSYS-FLUENT software was employed to solve and analyze the governing equations applying the SIMPLE algorithm with PRESTO and QUICK methods to discretize the momentum and energy equations, respectively. The convergence criteria are set to 10^{-4} for continuity and 10^{-6} for the momentum and energy equations. Furthermore, it should be noted that different grids and sizes of time-step were also performed to obtain the results independently from the grid and time step size. It should be noted that due to transient analysis of the phase-change problem, the convergence of all the governing equations at each time step should be checked and satisfied for different grid sizes with the given time steps which are performed in this study.

The heat recovery or solidification rate over 16 h was considered as the criteria to find the mesh independently from the number of cells and size of time step. First, different node numbers of 35,122, 52,682 and 105,364 are evaluated considering a time step size of 0.2 for the case with a uniform distribution of the tubes. The results show that the average solidification rate is 53.43, 52.89, and 52.74 for the system with 35122, 52,682, and 105,364 nodes, respectively. Therefore, the mesh with 52,682 nodes is selected for further analysis since the difference in the solidification rate between this case and the case with 105,364 nodes is less than 0.5%. Figure 2 shows the mesh of the selected case for the middle part of the domain. It should be noted that a uniform mesh is generated in all of the domains considering an edge sizing of 0.66 mm for all the walls of the domain. Different time step sizes of 0.1, 0.2, and 0.4 s are also studied to find the results independently from the size of the time step for the selected mesh. The results showed almost similar solidification rates of 53.01, 52.89, and 52. 55 for different sizes of time steps, and therefore the size of the time step was also selected as equal to 0.2 s. It should be noted that for each simulation, a high spec PC was used using four CPUs in parallel with a base speed of 2.39 GHz. For the case with uniform distribution of the tubes, the simulation of the solidification process for 16 h took 43 h and 29 min.

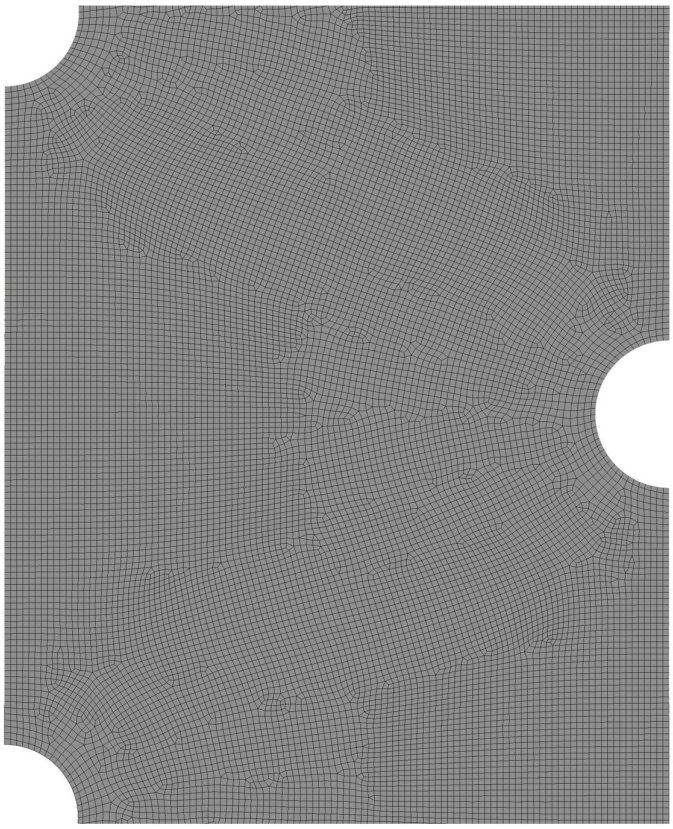

Figure 2. The mesh with 52,682 nodes in the middle of the domain.

The investigation of Mat et al. [69] was regenerated to verify the employed numerical simulation in the present study for a phase-change problem. Mat et al. [69] examined a finned-type dual-pipe LHS numerically and experimentally using organic PCM. The comparison is illustrated in Figure 3 between the numerical and practical results of the mean temperature and the numerical data of liquid fraction belongs to the study of Mat et al. with the present numerical study, which shows an excellent agreement.

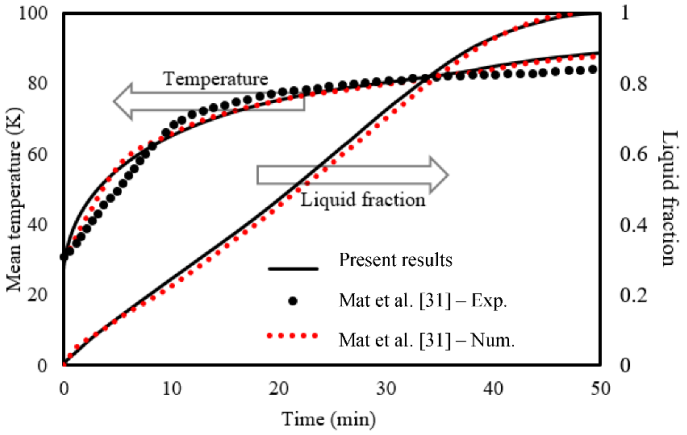

Figure 3. Code verification for a phase-change problem using the experimental data of Mat et al. [69].

To validate the accuracy during the solidification process, the present study is compared with the experimental work of Al-Abidi et al. [15]. They investigated the PCM temperature variation in a triple-tube PCM heat exchanger with fins. As observed in Figure 4, the comparison of the PCM average temperature of the present study are in good agreement with the experimental study of Al-Abidi et al. [15] showing the accuracy of the present model for the solidification process.

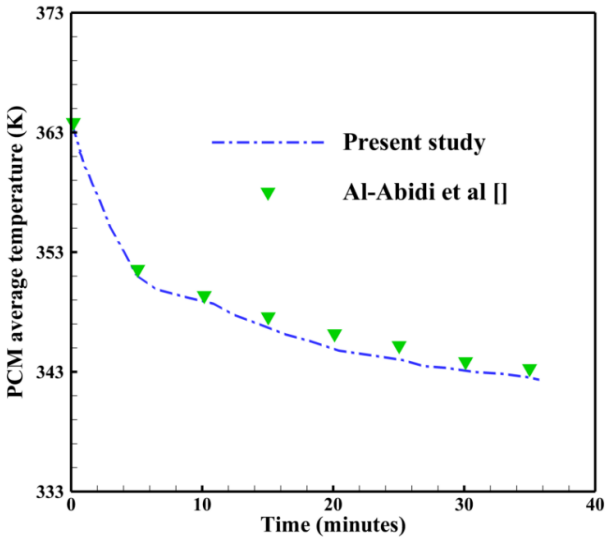

Figure 4. Code verification during the solidification process using the experimental study of Al-Abidi et al. [15].

5. Results and Discussion

Several simulations were run based on the model presented in the preceding section to identify the best design of the PCM-based TES unit with multiple tubes carrying the heat-transfer fluid (HTF). The impacts of natural convection on the thermofluidic performance of PCM during the energy discharging mode were discussed and revealed. During the discharging mode, a buoyancy-driven flow is particularly induced in the top portions of the PCM domain. This is due to the fact that hot liquid PCM tends to travel upward, and warm streams always settle at the top of the enclosure; hence, the density of the warm liquid PCM is lower than that of the cold solid PCM. In order to better profit from the nonuniformity of natural convection along the vertical direction, the energy storage units consisting of multiple HTF tubes must be properly designed. Therefore, the placement height of the HTF tubes was adopted as a design parameter in this analysis. There are three geometrical design variables, as shown in Figure 1, which are HL0, HL1, HL2, and HL3. Therefore, four different arrangements were considered, and the details are summarized in Table 2.

Table 2. The geometric parameters of the different tube arrangements adopted in the cases studied.

Description	HL_0 (Height of the First Tube)	$HL_{1,2,3}$ (Height of the Second, Third and Fourth Tube)
P7	$20 + D/2$	$71.73 + D$
P7-top	$20 + D/2$	$40 + D$
P7-mid	$67.06 + D/2$	$40 + D$
P7-bottom	$20 + D/2$	$40 + D$

To better understand the geometric parameters, Figure 5 displays the different proposed geometries presented in Table 2.

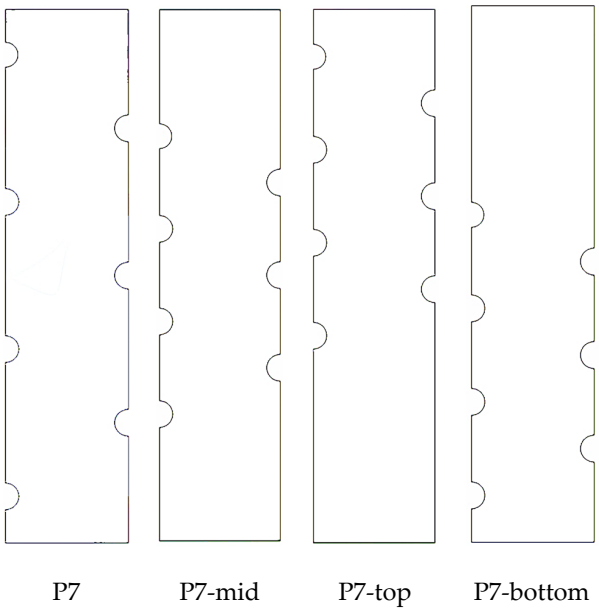

Figure 5. The schematic of the studied geometries presented in Table 2.

5.1. Natural Convection Impact for the Different Pipe Arrangements

The effects of applying different tube arrangements on the liquid-fraction contours, temperature distribution, velocity field, and streamlines over four different solidification durations (t = 4, 8, 12, and 16 h) are shown in Figures 6–8, respectively. There is a temperature gradient created in the early durations of the solidification when heat is primarily transferred via conduction between the cooler tube walls and the nearby solidifying fronts (marked in green) that surround the solid zone. Thereby, a buoyant force is generated which, once a sufficient amount of time has passed, becomes able to overpower the viscous force and aids in the creation of a buoyancy-driven flow at the top portion. During the first duration (t = 4 h), natural convection takes over as the primary heat transfer mechanism, allowing a delay in solidifying the PCM at the upper portions of the system. The size of the unsolidified PCM part (the red zone) is greatly dependent on the type of the tube arrangement being used. In all time durations, the size of the unsolidified PCM as compared between the four tube distribution cases becomes smaller as the tube arrangement moves from the reference case of the uniform tube distribution, i.e., P-7. As can be seen from Figure 6, the maximum delay in the solidification evolution was in the case of P7-bottom. This implies that moving the HTF tubes from the uniform distribution would negatively affect the potential for propagation of solidification in the liquid zones. Therefore, solidification takes a longer duration to be terminated, especially in the case of the bottom tube arrangement (P7-bottom). This is attributed to the dominance of local convection over conduction in the upper portions of the domain, allowing slower solidification rates in these zones.

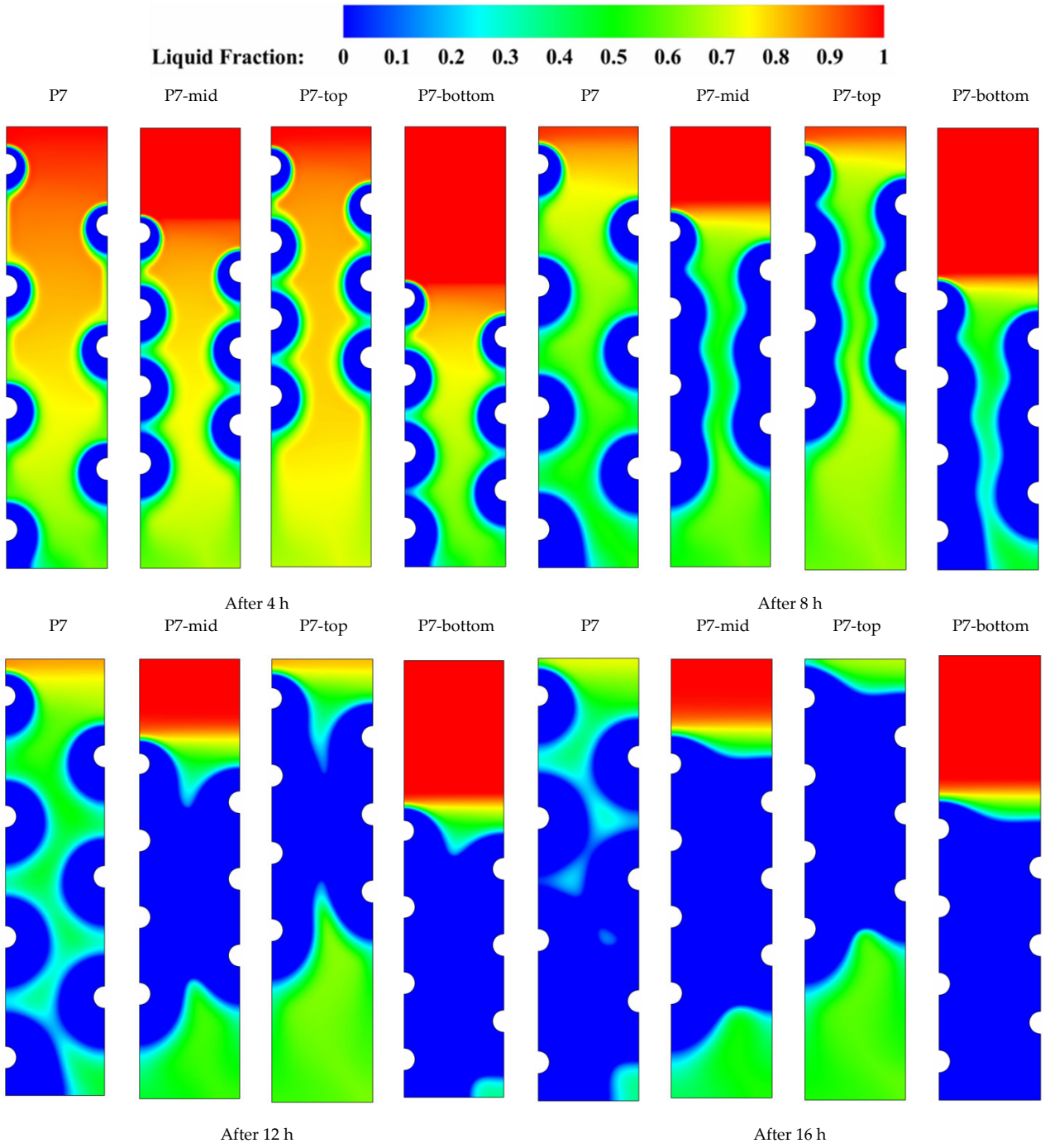

Figure 6. Contours of the liquid-fraction evolution for the studied tube arrangements over different durations of PCM solidification.

Figure 7 shows the temperature distribution over different time durations for the studied pipe arrangements. Heat conduction dominates the heat transfer process during the earlier stage of solidification (t = 6 h). A considerable variance in the color of isotherms is noted as time passes, and the pipe distribution held out the reference case of uniform pipe distribution. For example, comparing the isotherms in the case of bottom distribution (the fourth column) to the base case (the first column) shows that the isotherms depart from uniformity in color especially in the upper part due to the temperature gradients

generated with the presence of buoyancy-driven flow in these portions. This discoloration is a sign for the influencing convection contribution in the overall heat transfer process. However, this convection contribution results in a delay in solidification completion, which is the status where the temperature balance between the HTF and the PCM exists. Therefore, decreasing or increasing the distance between the multiple HTF tubes does not bring any improvements to the solidification behavior of PCM compared to that in the base case of uniform tube distribution. Further, the convective heat transfer is affected more by decreasing the distance between the tubes (the case of P7-mid) or moving the HTF tube to lower positions (the case of P7-bottom). The corresponding streamlines and velocity fields that are shown in Figure 8 confirm that during the time period (t = 8 h), the shift of tube positions from their reference positions in the case of P-7 only further boost the heat transport by convection in the liquid PCM. For example, moving the positions of HTF tubes to the bottom (P7-bottom) drives the velocity vectors to show faster movement with the formation of multiple rotating cells at the top of the domain. This helps the rotating cells to look more crowded, indicating evolution of a relatively stronger convection role which gradually decreases when moving to the bottom, as can be seen in Figure 8 when comparing the cases of P7-mid, P7-top, and P7-bottom to the base case of P7.

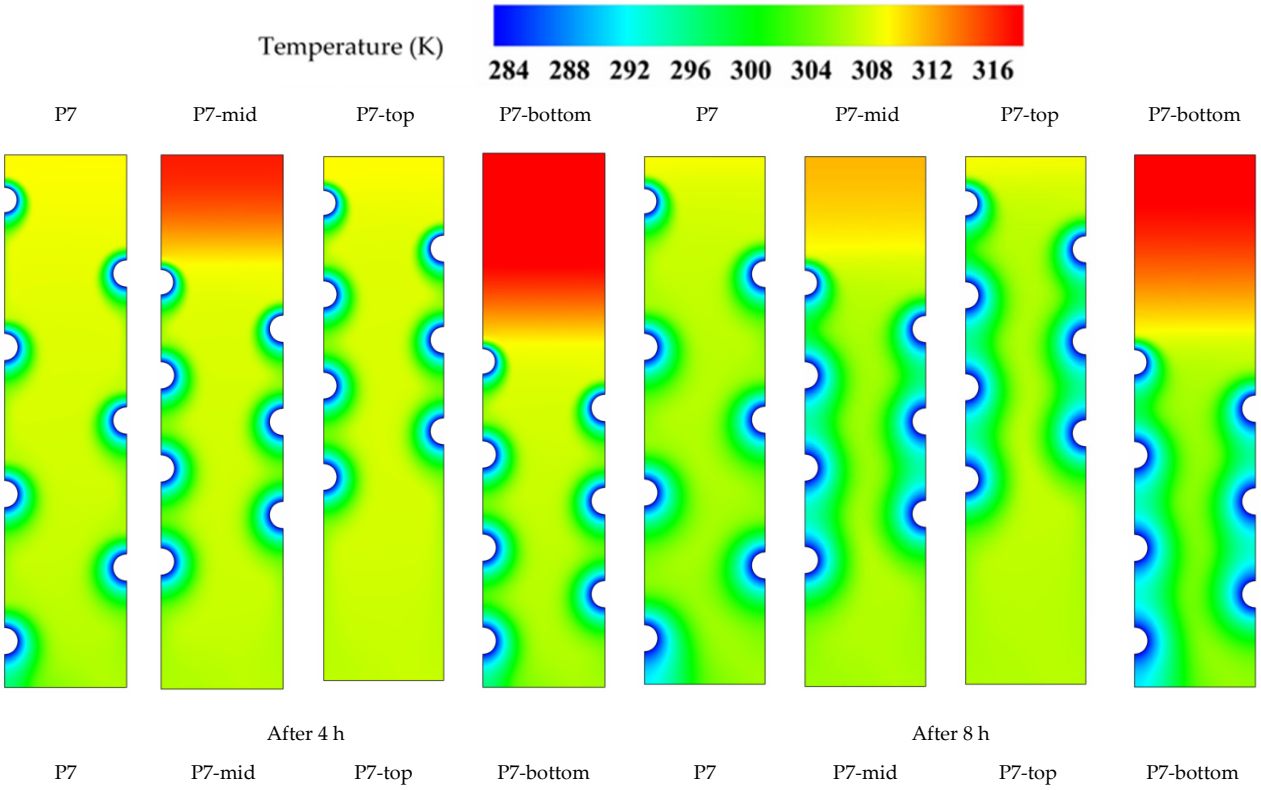

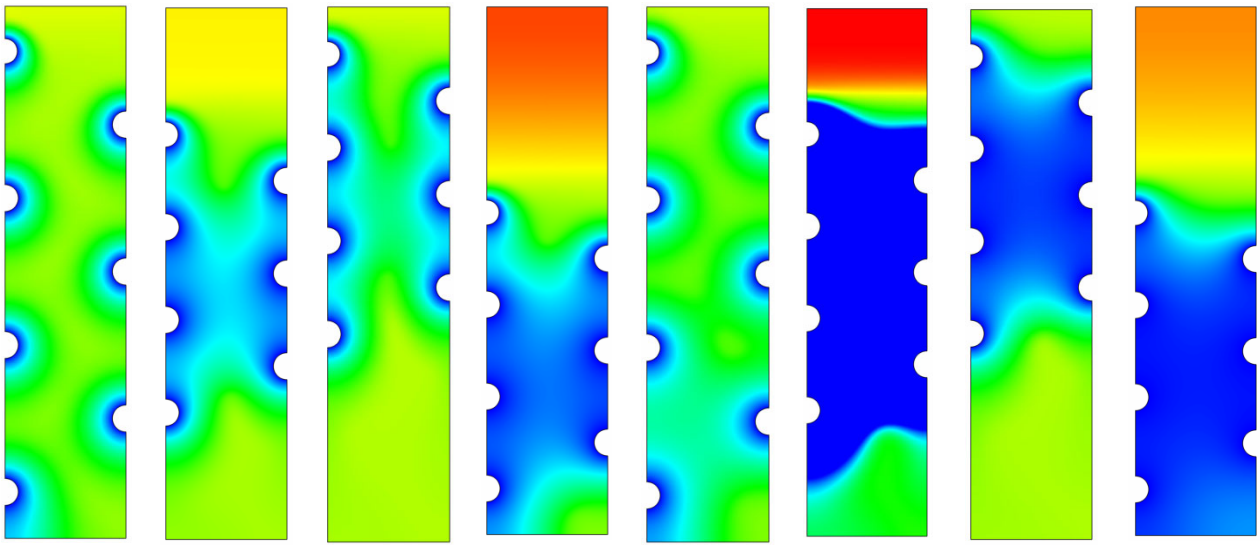

Figure 7. Contours of the temperature distribution for the studied tube arrangements over different durations of PCM solidification.

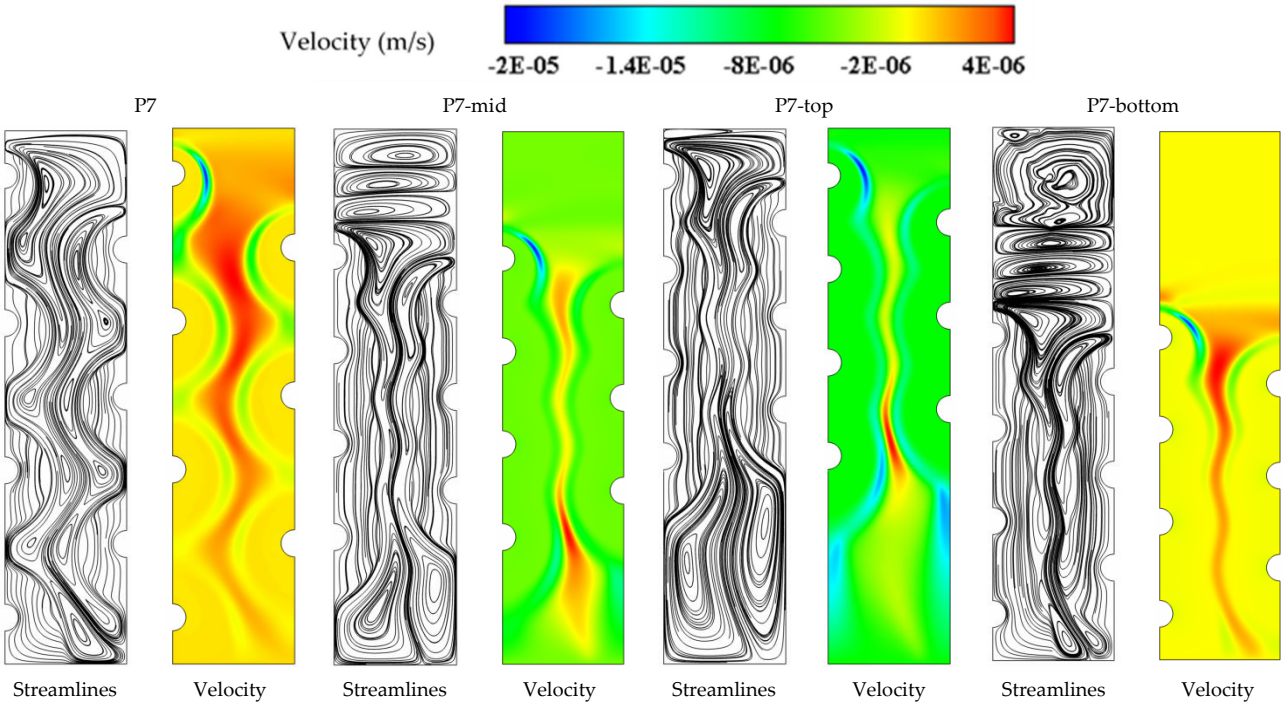

Figure 8. Contours of the velocity field and streamlines for the studied tube arrangements after 8 h of PCM solidification.

Figures 9 and 10 compare the time histories for liquid-fraction evolution and average temperature behavior in the cases of P-7, P7-mid, P7-top, and P7-bottom, respectively. As seen in Figure 9, maintaining a uniform distribution of HTF tubes in the case of P-7 typically provides better heat removal from the PCM. Meanwhile, decreasing the distances between tubes (P7-mid) or moving the tube positions up (P7-top) or down (P7-bottom) will affect the potential of HTF tubes to maintain good heat removal rates from the PCM. However, the lowest removal rate is recorded in the case of P7-bottom due to the high

convection rates in the upper part of the domain, which leads to relatively lower solidification rates. Data from Table 3 also confirm that changing the uniform distribution of the tubes reduces the heat removal rate from 52.89 W to 14.85 W, 22.05 W, and 24.55 W when the tube placements are altered to be clustered at the bottom, mid, or top of the domain, respectively. This results in a 72, 58, and 54% drop in the heat removal rate, respectively.

The data in Figure 10 show that applying a uniform distribution of tubes helps to maintain the PCM temperature lower throughout the solidification process. Changing the tube placements does not introduce a significant improvement in the PCM temperature behavior for the early duration (i.e., for $t \leq 35{,}000$ s) of solidification. The average temperature reaches its minimal value in a relatively shorter period when the distribution of the tubes is kept as uniform as that in the case of P-7 compared to other cases. However, the temperature behavior curves for later durations ($t > 35{,}000$ s) feature noticeable inflection points where the average PCM temperature appears to be significantly declined after this point in all cases except the base case of P-7. The reason is that the convective heat transfer during the final duration has a limited ability to accelerate the solidification of residual PCM after the inflection point. It should be noted that the heat removed by convection during the early periods is later stored as sensible heat in the unsolidified parts of PCM, resulting in a quick fall in the PCM average temperature after the inflection point, as seen in Figure 10. So, the inflection point can directly measure the solidifying performance, and the lower the average PCM temperature at the inflection point, the faster the solidifying rate.

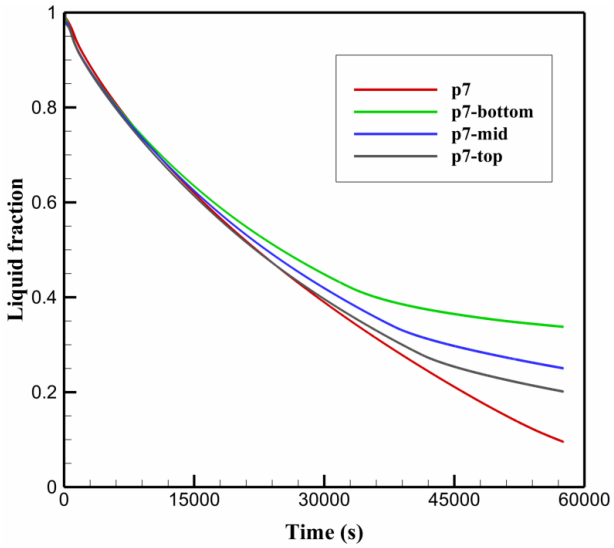

Figure 9. The time-wise liquid-fraction evolution profiles for the PCM solidification with different tube arrangements.

Table 3. The heat removal rate during the PCM solidification with different tube arrangements.

Cases	P7	P7-Bottom	P7-Mid	P7-Top
The heat removal rate after 16 h (watt)	52.89	14.850	22.051	24.545

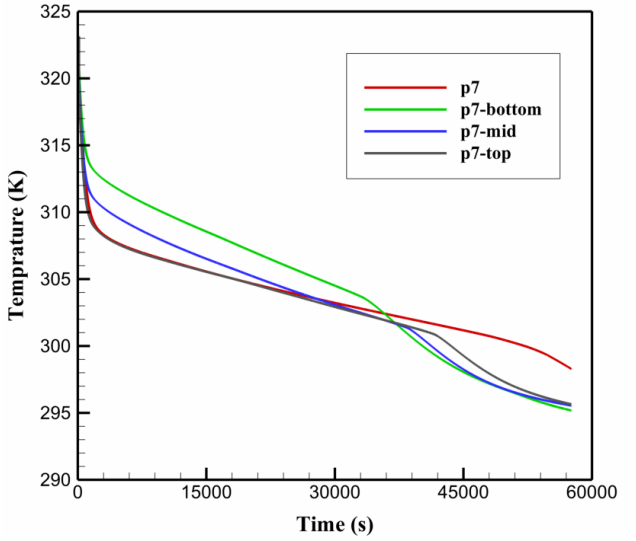

Figure 10. The time-wise average temperature profiles for the PCM solidification with different tube arrangements.

5.2. Optimization of the Tube Placement

According to the results of Section 5.1, the rates of natural convection in the top portions of the PCM domain are much higher than those in the bottom portions. As a result, a greater proportion of the remaining liquid PCM collects near the top. Moving the tube set closer to the top wall is the remedy to resolve the issue suggested in this section. The thermal performance of PCM is therefore examined with three tube arrangements. These arrangements are: P7 (the base arrangement), P7-1 (the arrangement where the tube set is moved closer to the top wall), and P7-2 (the arrangement where the tube set is stacked to the top wall). Figure 11 shows the contours of the liquid fraction at t = 4, 8, 12 and 16 h. It can be observed that for the three cases of P7, P7-1, and P7-2, the solidification is highly nonuniform; hence, more liquid PCM remains at the top due to the strong role of natural convection in this zone. Meanwhile, the size of the solidified layers (blue zones) looks almost the same among the three cases. However, as time passes, the solidifying fraction at the top portion slightly increases in the case of P7-1 compared to the other cases. The good tube placement of this case provides better heat diffusion through the PCM; thus, a faster discharging rate is achieved. As shown in Table 4, changing the arrangement of the tubes in the top portion increases the heat removal rate from 61.76 W to 68.75 W, and 67.75 W when the tube placement is altered from the base case (P7) to the new cases (P7-1 and P7-2), respectively. This results in a 10 and 12% increase in the heat removal rate, respectively. Table 4 also shows that the solidifying time is reduced from 110,775 s to 99,304 s and 100,488 s to provide time savings of about 11% and 9% when the tube placement is altered from the base case (P7) to the new cases (P7-1 and P7-2), respectively. This indicates that the tube arrangement of P7-1 is the optimum between the cases of uniform tube distribution.

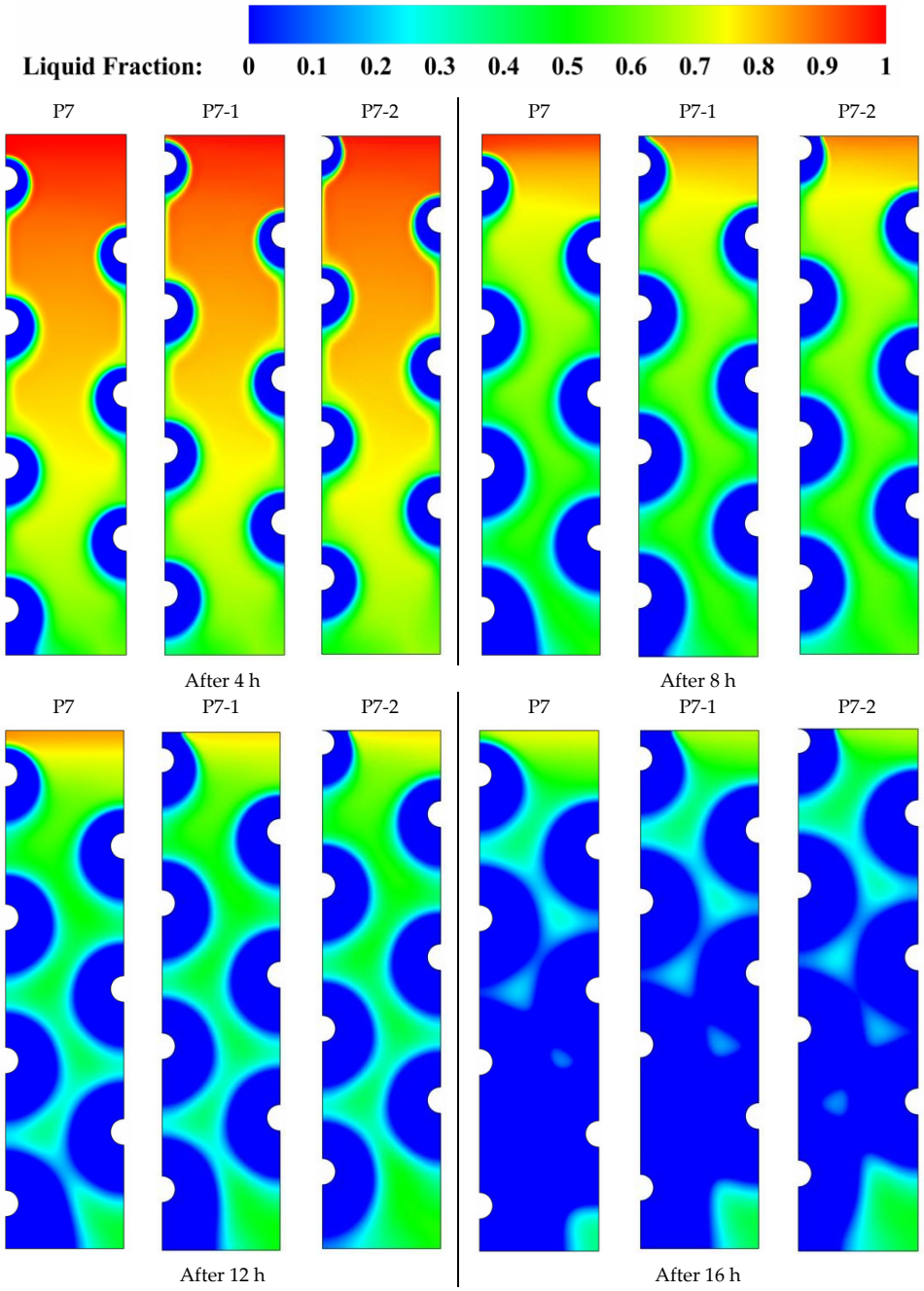

Figure 11. Contours of the liquid fraction for the three different uniform tube arrangements over different solidification durations.

Table 4. The heat removal rate and solidifying time for different uniform tube arrangements.

Cases	P7	P7-1	P7-2
Heat removal rate (W)	61.76	68.75	67.75
Solidifying time (s)	110,775	99,304	100,488

Figure 12 shows the isotherm contours for the three cases of P7, P7-1, and P7-2 along the time durations of t = 4, 8, 12 and 16 h. A significant variance in the color of the isotherms is noted; hence, the heat conduction dominates the heat transfer process during the earlier stage of solidification (t = 4 h). As time passed to t = 12 and 16 h, the isotherms

seem to be almost uniform in color across all parts of the domain, especially in the case of P7-1 as compared to other cases. This color uniformity is a sign of mitigating the effects of natural convection due to the modification conducted in the tube arrangement at the top portion. Therefore, moving the multiple HTF tubes closer to the top wall does inspire the PCM parts to solidify faster than that in the base case of P7. The corresponding streamlines and velocity fields shown in Figure 13 confirm that during the time period (t = 8 h), the little shift of tube positions up from their reference positions in the case of P-7 can further boost the heat removal process to be less convection dominated in the domain's upper portions. For example, moving the placements of the HTF tubes closer to the top wall, as in the case of (P7-1), causes the PCM molecules to move at lower velocities, resulting in the development of smaller rotating cells at the top of the domain. This makes the rotating cells appear larger and less crowded, indicating the evolution of such a relatively smaller convection role as moving to the top, as can be seen in Figure 13 when comparing the cases of P7-1 and P7-2 to the base case of P7.

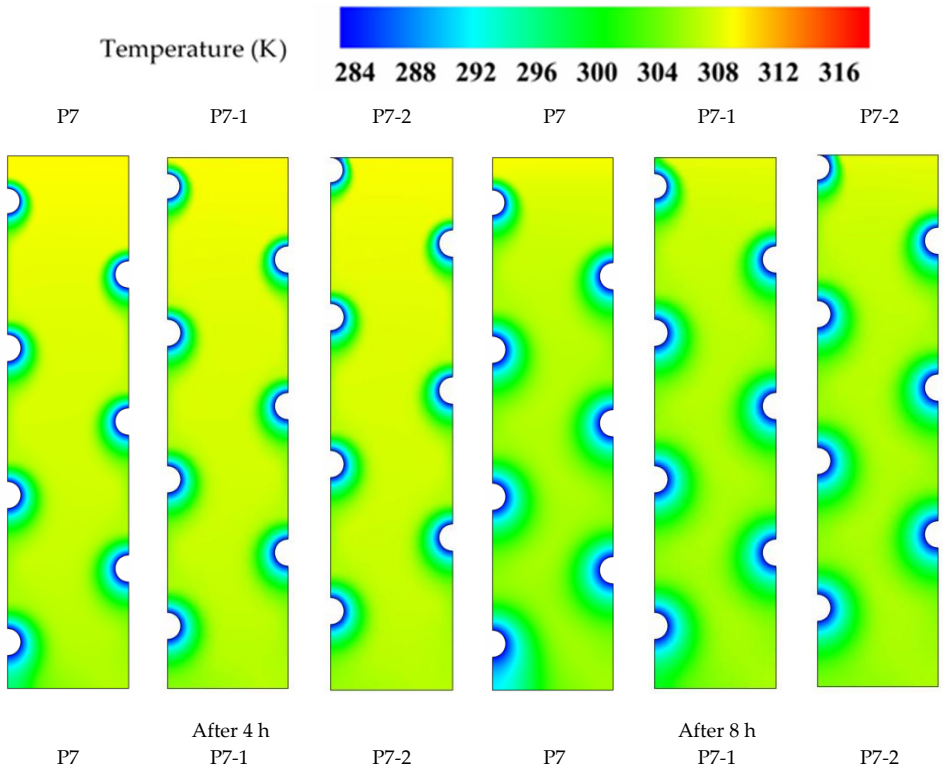

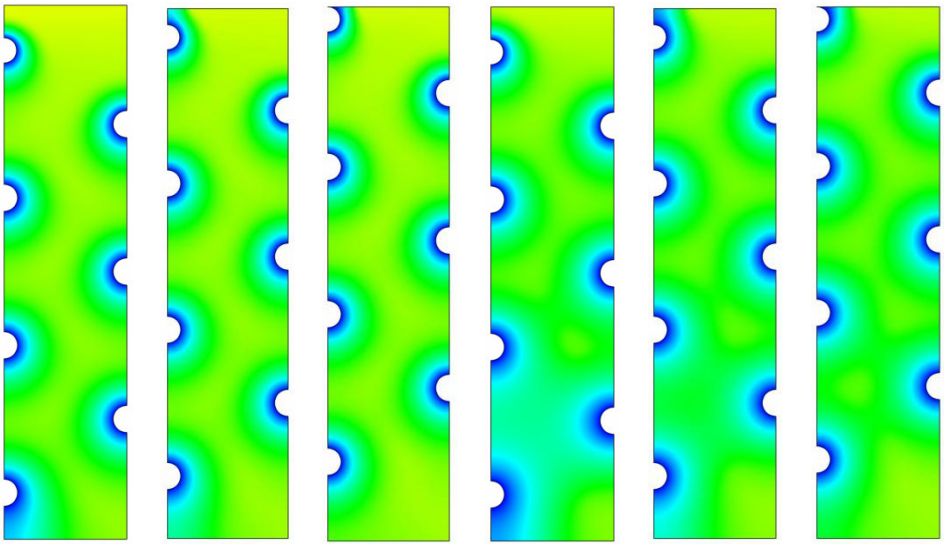

Figure 12. Contours of the temperature distribution for the three different uniform tube arrangements over different solidification durations.

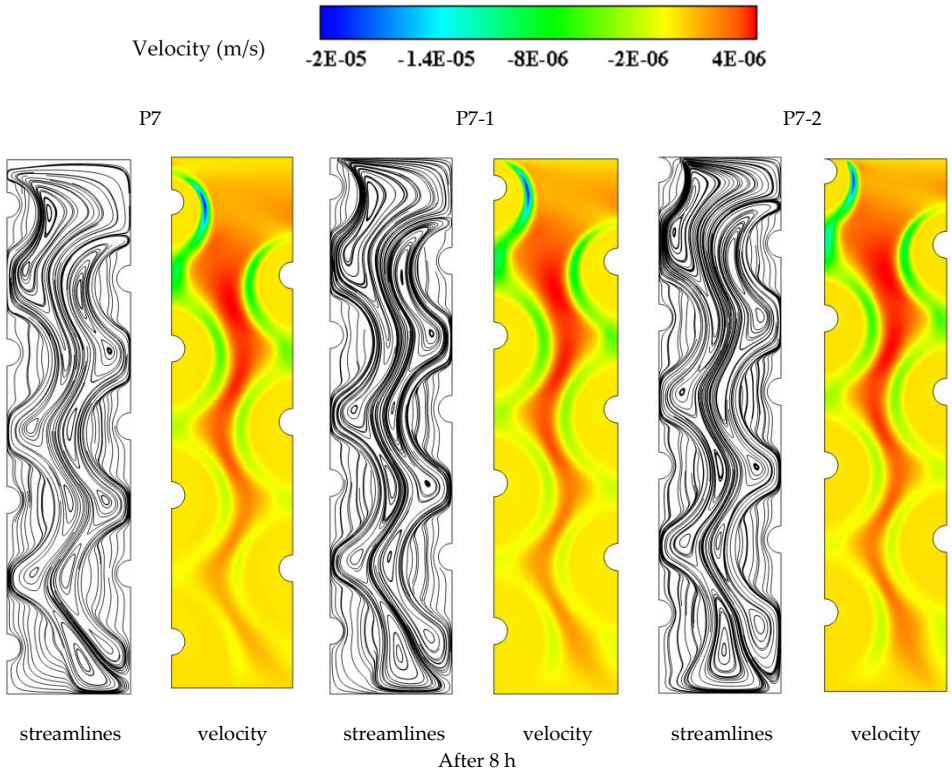

Figure 13. Contours of the velocity field and streamlines for the three different uniform tube arrangements after 8 h of PCM solidification.

5.3. Impact of the Inlet HTF Temperature

The impact of varying the inlet HTF temperature is examined considering the base case of uniform distribution (P-7). In this analysis, three temperatures of the HTF, namely THTF = 10, 15, and 20 °C, are considered so that the new cases are referred to as P7-10, P7-

15, and P7-20. The liquid-fraction evolution and isotherm distribution over two durations (t = 8 and 16 h) for the cases of P7-10, P7-15, and P7-20 are illustrated in Figures 14 and 15, respectively. Over the 8 h running process, the generated solid layers (blue zones in Figure 13) grow faster as the HTF temperature declines. This effect is more noticeable at the lower sections of the domain due to the relatively higher heat removal rates by heat conduction. This is due to the fact that when a greater HTF temperature is employed, the temperature difference relative to the PCM solidification point drops significantly. The corresponding isotherms in Figure 15 look similar to each other near the bottom of the domain. This helps increase heat removal rate and improve overall storage performance of the system during the subsequent duration.

After 16 h of solidification, the majority of the PCM in the case of P-7 is solidified, with only a small portion remaining uncodified at the top of the domain due to the stronger buoyancy effect in this zone. However, the temperature distribution in the case of P7-10 tends to be more even compared to the other two cases, except at some areas at the top due to the still-effective role of natural convection, as stated above. This implies that the temperature field is affected more by conduction than by natural convection if lower HTF temperatures are employed. Therefore, the temperature difference between the tube walls and the solidification temperature point is the primary driving force for the heat removal process. This results in more uniform temperature distribution during solidification and improved thermal diffusion across major parts of the PCM domain. This scenario is more clearly seen in the cases of P7-15 and P7-20, which represent HTF temperatures of 15 and 20 degrees Celsius, respectively.

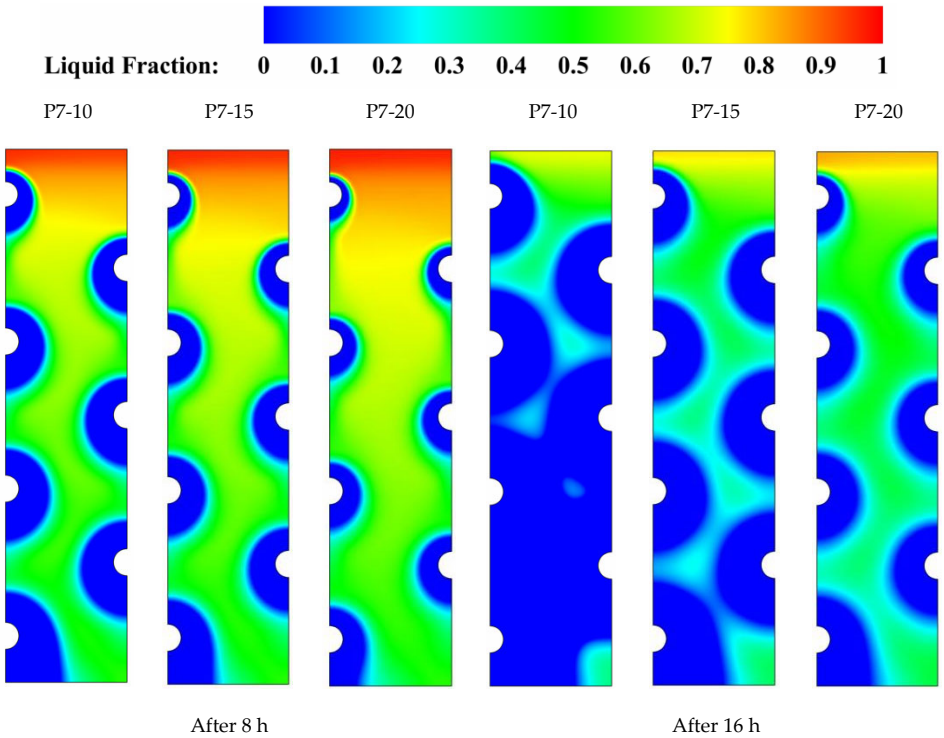

Figure 14. Contours of the liquid fraction for the base case of uniform tube arrangement at three different HTF temperatures.

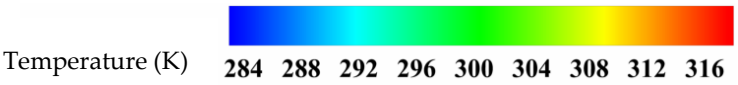

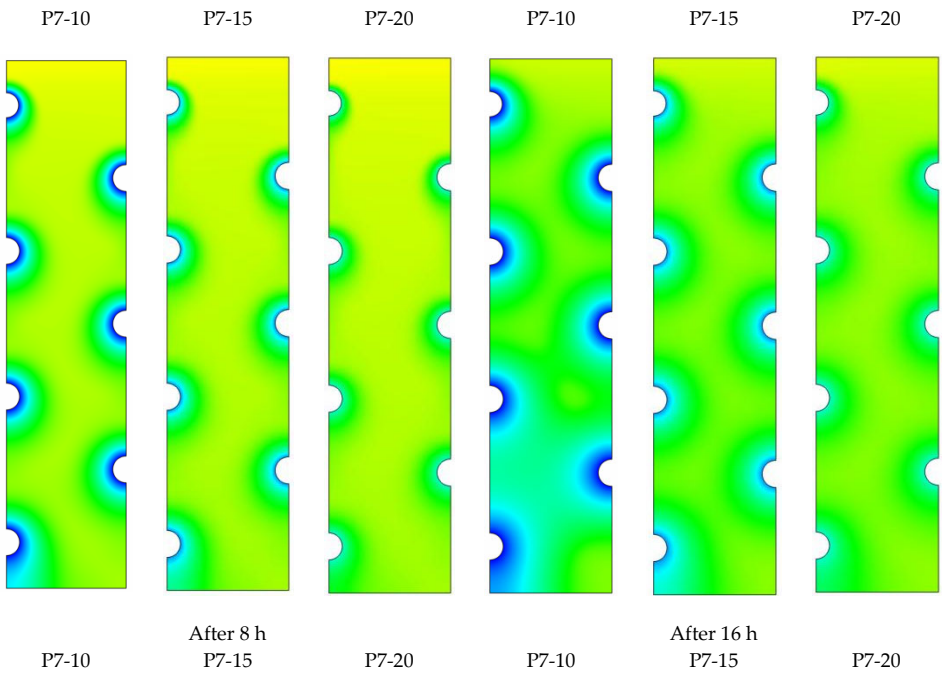

Figure 15. Contours of the liquid fraction for the base case of uniform tube arrangement at three different HTF temperatures.

Figure 16 compares the effect of increasing the inlet HTF temperature on the transient evolution of the liquid fraction and average PCM temperature profile for P7-10, P7-15, and P7-20, which correspond to THTF = 10, 15, and 20 °C, respectively. Data from this figure indicate that as lower HTF temperatures are employed, the value of the liquid fraction and the average PCM temperature linearly increases. So, decreasing the HTF temperature, in other words, promotes a higher cooling impact on the PCM side. This is primarily because using a colder HTF allows for a faster solidification rate of PCM. This trend appears to be more obvious as the process comes closer to the completion of solidification. As explained earlier, the contribution of conduction in the heat removal process becomes more effective and dominating over the contribution of natural convection within the final duration (t > 60,000 s) of solidification. Data from Table 5 show that a PCM with an HTF temperature of 10 °C solidifies at a rate of 52.89 W, but this rate declines to 48.91 and 40.36 W at THTF = 15 and 20 °C, respectively. Therefore, when the HTF temperature is decreased from 20 to 15 and 10 °C, the heat removal rate can be increased by around 21% and 32%, respectively.

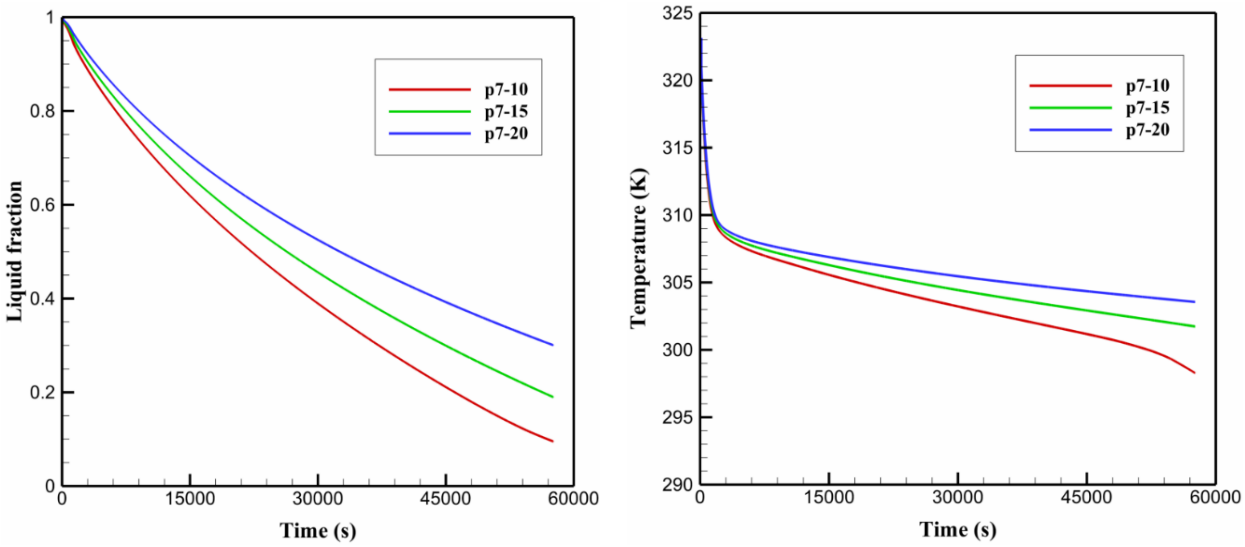

(**a**) (**b**)

Figure 16. The time-wise liquid fraction (**a**) and average temperature profiles (**b**) for the PCM solidification with uniform tube arrangement at three different HTF temperatures.

Table 5. The heat removal rate during the PCM solidification with uniform tube arrangement at three different HTF temperatures.

Cases	P7-10	P7-15	P7-20
Heat removal rate after 16 h (watt)	52.89	48.91	40.36

6. Conclusions

A geometrical model of an LHTES system cooled by HTF channels was analytically examined. The design of the LHTES contained seven HTF channels distributed in different locations in the system for different cases, including uniform distribution of the tubes as well as non-uniform distribution, i.e., tubes concentrated at the bottom, middle, and the top part of the shell. The effect of the channels' positions on the solidification process in the LHTES system was referred to, utilizing the development of the solid part, solidification maps, streamlines, and isotherms. It should be stated that such an enhancement is achieved without extra costs, since no extra material should be used in the manufacture of an LHTES system. Changing the uniform distribution of the tubes reduces the heat removal rate from 52.89 W to 14.85 W, 22.05 W, and 24.55 W when the tube placements are altered to be clustered at the bottom, middle, or top of the domain, respectively. The solidifying time is reduced from 110,775 s to 99,304 s and 100,488 s to provide time savings of about 11% and 9% when the tube placement is altered from the base case (P7) to the new cases (P7-1 and P7-2), respectively. The heat removal decreases with increasing the inlet temperature of the HTF, whereas it reduces by 7.5%, and 23.7% when the inlet temperature of the HTF increases from 10 °C to 15 °C and 20 °C, respectively. The current work states that special attention should be paid to the arrangement of the tubes as it enhances the discharging process focusing natural convection effect in TES. The distance between the channels could be an additional important geometrical factor, as it essentially could control initial solidified regions and the interface of general movement flows. The study of the space between the channels could be a topic for future studies.

Author Contributions: Conceptualization, J.M.M. and P.T.; methodology, P.T.; software, P.T.; validation, P.T.; formal analysis, M.E.T., J.M.M., H.I.M., H.S.M., A.E., R.B.M., P.T. and W.Y.; investigation, M.E.T., J.M.M., H.I.M., H.S.M., A.E., R.B.M., P.T. and W.Y.; resources, R.B.M., P.T. and W.Y.; writing—original draft preparation, M.E.T., J.M.M., H.I.M., H.S.M., A.E., R.B.M., P.T. and W.Y.;

writing—review and editing, M.E.T., J.M.M., H.I.M., H.S.M., R.B.M., A.E., P.T. and W.Y.; visualization, J.M.M., H.I.M. and P.T.; supervision, P.T. All authors have read and agreed to the published version of the manuscript.

Funding: This research received no external funding.

Institutional Review Board Statement: Not applicable.

Informed Consent Statement: Not applicable.

Data Availability Statement: The data will be available on request.

Conflicts of Interest: The authors declare no conflict of interest.

Nomenclature

A_m	The mushy zone constant	u	Velocity component in x direction (m/s)
C	Inertial coefficient	v	Velocity component in y direction (m/s)
C_p	PCM specific heat (J/kgK)	$\vec{V}$	Velocity vector (m/s)
D	Pipe diameter (mm)	x	x direction
g	Gravitational acceleration (m/s^2)	y	y direction
K	thermal conductivity (W/mK)		
L_f	Latent heat of fusion (J/kg)	**Greek Symbols**	
H	Total entalhpy (mm)	β	Thermal expansion coefficient (1/K)
h	Sensible heat entalhpy (mm)	λ	Liquid fraction
m	PCM mass (kg)	μ	Dynamic viscosity (kg/ms)
P	Pressure (Pa)	ρ	Density (kg/m^3)
$\dot{Q}$	Solidification rate (J)	ΔH	Latent heat entalhpy (mm)
t_m	Solidification time (s)	**Subscripts**	
T	Temperature (K)	m	Melting
T_m	Melting point temperature (K)	L	Liquid
		S	Solid

References

1. Guo, X.; Liu, J.; Dai, L.; Liu, Q.; Fang, D.; Wei, A.; Wang, J. Friction-wear failure mechanism of tubing strings used in high-pressure, high-temperature and high-yield gas wells. *Wear* **2021**, *468*, 203576.
2. Zhao, X.; Gu, B.; Gao, F.; Chen, S. Matching model of energy supply and demand of the integrated energy system in coastal areas. *J. Coast. Res.* **2020**, *103*, 983–989.
3. Höök, M.; Tang, X. Depletion of fossil fuels and anthropogenic climate change—A review. *Energy Policy* **2013**, *52*, 797–809, doi:10.1016/j.enpol.2012.10.046.
4. Khan, Z.; Khan, Z.A.; Sewell, P. Heat transfer evaluation of metal oxides based nano-PCMs for latent heat storage system application. *Int. J. Heat Mass Transf.* **2019**, *144*, 118619.
5. Zhang, L.; Zheng, H.; Wan, T.; Shi, D.; Lyu, L.; Cai, G. An integrated control algorithm of power distribution for islanded microgrid based on improved virtual synchronous generator. *IET Renew. Power Gener.* **2021**, *15*, 2674–2685.
6. Jiang, T.; Liu, Z.; Wang, G.; Chen, Z. Comparative study of thermally stratified tank using different heat transfer materials for concentrated solar power plant. *Energy Rep.* **2021**, *7*, 3678–3687.
7. Zhang, J.; Wu, W.; Li, C.; Yang, M.; Zhang, Y.; Jia, D.; Hou, Y.; Li, R.; Cao, H.; Ali, H.M. Convective heat transfer coefficient model under nanofluid minimum quantity lubrication coupled with cryogenic air grinding Ti–6Al–4V. *Int. J. Precis. Eng. Manuf.-Green Technol.* **2021**, *8*, 1113–1135.
8. Ghalambaz, M.; Eisapour, A.H.; Mohammed, H.I.; Islam, M.S.; Younis, O.; Sardari, P.T.; Yaïci, W. Impact of Tube Bundle Placement on the Thermal Charging of a Latent Heat Storage Unit. *Energies* **2021**, *14*, 1289.
9. Da Cunha, J.P.; Eames, P. Thermal energy storage for low and medium temperature applications using phase change materials–a review. *Appl. Energy* **2016**, *177*, 227–238.
10. Khan, Z.; Khan, Z.; Ghafoor, A. A review of performance enhancement of PCM based latent heat storage system within the context of materials, thermal stability and compatibility. *Energy Convers. Manag.* **2016**, *115*, 132–158, doi:10.1016/j.enconman.2016.02.045.
11. Cabeza, L.F.; Castell, A.; Barreneche, C.; de Gracia, A.; Fernández, A.I. Materials used as PCM in thermal energy storage in buildings: A review. *Renew. Sustain. Energy Rev.* **2011**, *15*, 1675–1695, doi:10.1016/j.rser.2010.11.018.
12. Keshtkar, M.M.; Talebizadeh, P. Multi-objective optimization of cooling water package based on 3E analysis: A case study. *Energy* **2017**, *134*, 840–849.
13. Xu, Q.; Wang, K.; Zou, Z.; Zhong, L.; Akkurt, N.; Feng, J.; Xiong, Y.; Han, J.; Wang, J.; Du, Y. A new type of two-supply, one-return, triple pipe-structured heat loss model based on a low temperature district heating system. *Energy* **2021**, *218*, 119569.

14. Dai, Z.; Xie, J.; Chen, Z.; Zhou, S.; Liu, J.; Liu, W.; Xi, Z.; Ren, X. Improved energy storage density and efficiency of (1 − x) $Ba_{0.85}Ca_{0.15}Zr_{0.1}Ti_{0.9}O_3$-x$BiMg_{2/3}Nb_{1/3}O_3$ lead-free ceramics. *Chem. Eng. J.* **2021**, *410*, 128341.
15. Al-Abidi, A.A.; Mat, S.; Sopian, K.; Sulaiman, M.; Mohammad, A.T. Experimental study of melting and solidification of PCM in a triplex tube heat exchanger with fins. *Energy Build.* **2014**, *68*, 33–41.
16. Shahsavar, A.; Goodarzi, A.; Mohammed, H.I.; Shirneshan, A.; Talebizadehsardari, P. Thermal performance evaluation of non-uniform fin array in a finned double-pipe latent heat storage system. *Energy* **2020**, *193*, 116800, doi:10.1016/j.energy.2019.116800.
17. Sajawal, M.; Rehman, T.-u.; Ali, H.M.; Sajjad, U.; Raza, A.; Bhatti, M.S. Experimental thermal performance analysis of finned tube-phase change material based double pass solar air heater. *Case Stud. Therm. Eng.* **2019**, *15*, 100543.
18. Memon, Z.Q.; Pao, W.; Hashim, F.M.; Ali, H.M. Experimental investigation of two-phase separation in T-Junction with combined diameter ratio. *J. Nat. Gas Sci. Eng.* **2020**, *73*, 103048.
19. Talebizadehsardari, P.; Mahdi, J.M.; Mohammed, H.I.; Moghimi, M.A.; Hossein Eisapour, A.; Ghalambaz, M. Consecutive charging and discharging of a PCM-based plate heat exchanger with zigzag configuration. *Appl. Therm. Eng.* **2021**, *193*, 116970, doi:10.1016/j.applthermaleng.2021.116970.
20. Mahani, R.B.; Mohammed, H.I. Phase Change Process in a Zigzag Plate Latent Heat Storage System during Melting and Solidification. *Molecules* **2020**, *25*, 4643, doi:10.3390/molecules25204643.
21. Mahdi, J.M.; Mohammed, H.I.; Talebizadehsardari, P.; Ghalambaz, M.; Majdi, H.S.; Yaïci, W.; Giddings, D. Simultaneous and consecutive charging and discharging of a PCM-based domestic air heater with metal foam. *Appl. Therm. Eng.* **2021**, *197*, 117408.
22. Talebizadeh Sardari, P.; Mohammed, H.I.; Mahdi, J.M.; Ghalambaz, M.; Gillott, M.; Walker, G.S.; Grant, D.; Giddings, D. Localized heating element distribution in composite metal foam-phase change material: Fourier's law and creeping flow effects. *Int. J. Energy Res.* **2021**, *45*, 13380–13396, doi:10.1002/er.6665.
23. Mohammed, H.I.; Talebizadehsardari, P.; Mahdi, J.M.; Arshad, A.; Sciacovelli, A.; Giddings, D. Improved melting of latent heat storage via porous medium and uniform Joule heat generation. *J. Energy Storage* **2020**, *31*, 101747, doi:10.1016/j.est.2020.101747.
24. Sardari, P.T.; Mohammed, H.I.; Giddings, D.; Walker, G.S.; Gillott, M.; Grant, D. Numerical study of a multiple-segment metal foam-PCM latent heat storage unit: Effect of porosity, pore density and location of heat source. *Energy* **2019**, *189*, 116108, doi:10.1016/j.energy.2019.116108.
25. Ghalambaz, M.; Mohammed, H.I.; Naghizadeh, A.; Islam, M.S.; Younis, O.; Mahdi, J.M.; Chatroudi, I.S.; Talebizadehsardari, P. Optimum Placement of Heating Tubes in a Multi-Tube Latent Heat Thermal Energy Storage. *Materials* **2021**, *14*, 1232, doi:10.3390/ma14051232.
26. Ghalambaz, M.; Mohammed, H.I.; Mahdi, J.M.; Eisapour, A.H.; Younis, O.; Ghosh, A.; Talebizadehsardari, P.; Yaïci, W. Intensifying the Charging Response of a Phase-Change Material with Twisted Fin Arrays in a Shell-And-Tube Storage System. *Energies* **2021**, *14*, 1619.
27. Bazai, H.; Moghimi, M.A.; Mohammed, H.I.; Babaei-Mahani, R.; Talebizadehsardari, P. Numerical study of circular-elliptical double-pipe thermal energy storage systems. *J. Energy Storage* **2020**, *30*, 101440, doi:10.1016/j.est.2020.101440.
28. Shahsavar, A.; Khosravi, J.; Mohammed, H.I.; Talebizadehsardari, P. Performance evaluation of melting/solidification mechanism in a variable wave-length wavy channel double-tube latent heat storage system. *J. Energy Storage* **2020**, *27*, 101063, doi:10.1016/j.est.2019.101063.
29. Gatea, M.A.; Jawad, H.A. Thermoplasmonic of single Au@ SiO_2 and SiO_2@ Au core shell nanoparticles in deionized water and poly-vinylpyrrolidonematrix. *Baghdad Sci. J.* **2019**, *16*, 376–381.
30. Singh, R.P.; Kaushik, S.; Rakshit, D. Melting phenomenon in a finned thermal storage system with graphene nano-plates for medium temperature applications. *Energy Convers. Manag.* **2018**, *163*, 86–99.
31. Mahdi, J.M.; Mohammed, H.I.; Talebizadehsardari, P. A new approach for employing multiple PCMs in the passive thermal management of photovoltaic modules. *Sol. Energy* **2021**, *222*, 160–174, doi:10.1016/j.solener.2021.04.044.
32. Mahdi, J.M.; Mohammed, H.I.; Hashim, E.T.; Talebizadehsardari, P.; Nsofor, E.C. Solidification enhancement with multiple PCMs, cascaded metal foam and nanoparticles in the shell-and-tube energy storage system. *Appl. Energy* **2020**, *257*, 113993, doi:10.1016/j.apenergy.2019.113993.
33. El Hasadi, Y.M.; Khodadadi, J. Numerical simulation of the effect of the size of suspensions on the solidification process of nanoparticle-enhanced phase change materials. *J. Heat Transf.* **2013**, *135*, 503–512.
34. Liu, X.; Mohammed, H.I.; Ashkezari, A.Z.; Shahsavar, A.; Hussein, A.K.; Rostami, S. An experimental investigation on the rheological behavior of nanofluids made by suspending multi-walled carbon nanotubes in liquid paraffin. *J. Mol. Liq.* **2020**, *300*, 112269, doi:10.1016/j.molliq.2019.112269.
35. Ju, Y.; Zhu, T.; Mashayekhi, R. Evaluation of Multiple Semi-Twisted Tape Inserts in a Heat Exchanger Pipe Using Al_2O_3 Nanofluid. **2021**, *11*, 150, doi:10.3390/nano11061570.
36. Talebizadehsardari, P.; Mohammed, H.I.; Mahdi, J.M.; Gillott, M.; Walker, G.S.; Grant, D.; Giddings, D. Effect of airflow channel arrangement on the discharge of a composite metal foam-phase change material heat exchanger. *Int. J. Energy Res.* **2021**, *45*, 2593–2609, doi:10.1002/er.5949.
37. Li, H.-W.; Gao, Y.-F.; Du, C.-H.; Hong, W.-P. Numerical study on swirl cooling flow, heat transfer and stress characteristics based on fluid-structure coupling method under different swirl chamber heights and Reynolds numbers. *Int. J. Heat Mass Transf.* **2021**, *173*, 121228.
38. Li, H.; Xu, B.; Lu, G.; Du, C.; Huang, N. Multi-objective optimization of PEM fuel cell by coupled significant variables recognition, surrogate models and a multi-objective genetic algorithm. *Energy Convers. Manag.* **2021**, *236*, 114063.

39. Dai, Z.; Xie, J.; Fan, X.; Ding, X.; Liu, W.; Zhou, S.; Ren, X. Enhanced energy storage properties and stability of Sr ($Sc_{0.5}Nb_{0.5}$) O_3 modified 0.65$BaTiO_3$-0.35 $Bi_{0.5}Na_{0.5}TiO_3$ ceramics. *Chem. Eng. J.* **2020**, *397*, 125520.
40. Ren, H.; He, M.; Lin, W.; Yang, L.; Li, W.; Ma, Z. Performance investigation and sensitivity analysis of shell-and-tube phase change material thermal energy storage. *J. Energy Storage* **2021**, *33*, 102040, doi:10.1016/j.est.2020.102040.
41. Pan, C.; Vermaak, N.; Wang, X.; Romero, C.; Neti, S. A fast reduced model for a shell-and-tube based latent heat thermal energy storage heat exchanger and its application for cost optimal design by nonlinear programming. *Int. J. Heat Mass Transf.* **2021**, *176*, 121479, doi:10.1016/j.ijheatmasstransfer.2021.121479.
42. Thyagarajan, A.; Shettigar, N.; Banerjee, D. Comparison of Thermal Performance of 3D Printed Shell and Tube Heat Exchanger With Commercial Plate Heat Exchanger for Thermal Energy Storage (TES) by Incorporating Phase Change Materials (PCM). In Proceedings of the Heat Transfer Summer Conference, Rosen Shingle Creek, Orlando, FL, USA, 25 September 2020; p. V001T011A012.
43. Maldonado, J.M.; Verez, D.; de Gracia, A.; Cabeza, L.F. Comparative study between heat pipe and shell-and-tube thermal energy storage. *Appl. Therm. Eng.* **2021**, *192*, 116974.
44. Yang, K.; Zhu, N.; Li, Y.; Du, N. Effect of parameters on the melting performance of triplex tube heat exchanger incorporating phase change material. *Renew. Energy* **2021**, *174*, 359–371.
45. Ghalambaz, M.; Mahdi, J.; Shafaghat, A.; Eisapour, A.; Younis, O.; Talebizadeh Sardari, P.; Yaïci, W. Effect of Twisted Fin Array in a Triple-Tube Latent Heat Storage System during the Charging Mode. *Sustainability* **2021**, *13*, 2685.
46. Al-Mudhafar, A.H.N.; Nowakowski, A.F.; Nicolleau, F.C.G.A. Enhancing the thermal performance of PCM in a shell and tube latent heat energy storage system by utilizing innovative fins. *Energy Rep.* **2021**, *7*, 120–126, doi:10.1016/j.egyr.2021.02.034.
47. Agyenim, F.; Hewitt, N.; Eames, P.; Smyth, M. A review of materials, heat transfer and phase change problem formulation for latent heat thermal energy storage systems (LHTESS). *Renew. Sustain. Energy Rev.* **2010**, *14*, 615–628.
48. Pakalka, S.; Valančius, K.; Streckienė, G. Experimental and Theoretical Investigation of the Natural Convection Heat Transfer Coefficient in Phase Change Material (PCM) Based Fin-and-Tube Heat Exchanger. *Energies* **2021**, *14*, 716.
49. Rathod, M.K.; Banerjee, J. Thermal performance enhancement of shell and tube Latent Heat Storage Unit using longitudinal fins. *Appl. Therm. Eng.* **2015**, *75*, 1084–1092, doi:10.1016/j.applthermaleng.2014.10.074.
50. Lohrasbi, S.; Gorji-Bandpy, M.; Ganji, D.D. Thermal penetration depth enhancement in latent heat thermal energy storage system in the presence of heat pipe based on both charging and discharging processes. *Energy Convers. Manag.* **2017**, *148*, 646–667, doi:10.1016/j.enconman.2017.06.034.
51. Esapour, M.; Hosseini, M.; Ranjbar, A.; Bahrampoury, R. Numerical study on geometrical specifications and operational parameters of multi-tube heat storage systems. *Appl. Therm. Eng.* **2016**, *109*, 351–363.
52. Darzi, A.A.R.; Jourabian, M.; Farhadi, M. Melting and solidification of PCM enhanced by radial conductive fins and nanoparticles in cylindrical annulus. *Energy Convers. Manag.* **2016**, *118*, 253–263.
53. Khan, Z.; Khan, Z.; Tabeshf, K. Parametric investigations to enhance thermal performance of paraffin through a novel geometrical configuration of shell and tube latent thermal storage system. *Energy Convers. Manag.* **2016**, *127*, 355–365, doi:10.1016/j.enconman.2016.09.030.
54. Hajizadeh, M.R.; Keshteli, A.N.; Bach, Q.-V. Solidification of PCM within a tank with longitudinal-Y shape fins and CuO nanoparticle. *J. Mol. Liq.* **2020**, *317*, 114188.
55. Du, K.; Calautit, J.; Eames, P.; Wu, Y. A state-of-the-art review of the application of phase change materials (PCM) in Mobilized-Thermal Energy Storage (M-TES) for recovering low-temperature industrial waste heat (IWH) for distributed heat supply. *Renew. Energy* **2021**, *168*, 1040–1057, doi:10.1016/j.renene.2020.12.057.
56. Zarei, M.J.; Bazai, H.; Sharifpur, M.; Mahian, O.; Shabani, B. The effects of fin parameters on the solidification of PCMs in a fin-enhanced thermal energy storage system. *Energies* **2020**, *13*, 198.
57. Gürtürk, M.; Kok, B. A new approach in the design of heat transfer fin for melting and solidification of PCM. *Int. J. Heat Mass Transf.* **2020**, *153*, 119671.
58. Tao, L.C. Generalized numerical solutions of freezing a saturated liquid in cylinders and spheres. *AIChE J.* **1967**, *13*, 165–169, doi:10.1002/aic.690130130.
59. Gortych, M.; Lipnicki, Z.; Weigand, B. An experimental and theoretical study of the solidification process of phase change materials in a horizontal annular enclosure. *Appl. Therm. Eng.* **2019**, *161*, 114140, doi:10.1016/j.applthermaleng.2019.114140.
60. Abdollahzadeh, M.; Esmaeilpour, M. Enhancement of phase change material (PCM) based latent heat storage system with nano fluid and wavy surface. *Int. J. Heat Mass Transf.* **2015**, *80*, 376–385, doi:10.1016/j.ijheatmasstransfer.2014.09.007.
61. Shahsavar, A.; Al-Rashed, A.A.A.A.; Entezari, S.; Sardari, P.T. Melting and solidification characteristics of a double-pipe latent heat storage system with sinusoidal wavy channels embedded in a porous medium. *Energy* **2019**, *171*, 751–769, doi:10.1016/j.energy.2019.01.045.
62. Choi, J.C.; Kim, S.D. Heat-transfer characteristics of a latent heat storage system using $MgCl_2 \cdot 6H_2O$. *Energy* **1992**, *17*, 1153–1164, doi:10.1016/0360-5442(92)90004-J.
63. Wang, P.; Li, D.; Huang, Y.; Zheng, X.; Wang, Y.; Peng, Z.; Ding, Y. Numerical Study of Solidification in a Plate Heat Exchange Device with a Zigzag Configuration Containing Multiple Phase-Change-Materials. *Energies* **2016**, *9*, 394.
64. Li, M.-J.; Li, M.-J.; Tong, Z.-X.; Li, D. Optimization of the packed-bed thermal energy storage with cascaded PCM capsules under the constraint of outlet threshold temperature. *Appl. Therm. Eng.* **2021**, *186*, 116473, doi:10.1016/j.applthermaleng.2020.116473.

65. Liang, H.; Niu, J.; Gan, Y. Performance optimization for shell-and-tube PCM thermal energy storage. *J. Energy Storage* **2020**, *30*, 101421, doi:10.1016/j.est.2020.101421.
66. GmbH, R.T. RT35 data sheet.
67. Talebizadeh Sardari, P.; Walker, G.S.; Gillott, M.; Grant, D.; Giddings, D. Numerical modelling of phase change material melting process embedded in porous media: Effect of heat storage size. *Proc. Inst. Mech. Eng. Part A J. Power Energy* **2019**. https://doi.org/10.1177/0957650919862974.
68. Xu, Y.; Ren, Q.; Zheng, Z.-J.; He, Y.-L. Evaluation and optimization of melting performance for a latent heat thermal energy storage unit partially filled with porous media. *Appl. Energy* **2017**, *193*, 84–95.
69. Mat, S.; Al-Abidi, A.A.; Sopian, K.; Sulaiman, M.Y.; Mohammad, A.T. Enhance heat transfer for PCM melting in triplex tube with internal–external fins. *Energy Convers. Manag.* **2013**, *74*, 223–236, doi:10.1016/j.enconman.2013.05.003.